RESEARCH ARTICLE

SAMRIDDHI Volume 13, Special Issue 2, 2021 Print ISSN : 2229-7111 Online ISSN : 2454-5767

Quantitative Analysis of Image Segmentation Algorithms: A Statistical Perspective

Prerna Pachunde[1*], Sudhir G. Akojwar[2]

[1,*] Deptt. of Electrical Engineering Department, Rajiv Gandhi College of Engineering Research and Technoology, Chandrapur India; e-mail : prerna.dahiwade@gmail.com

[2.] Deptt. of E&Tc, Government College of Engineering Chandpur, India.

ABSTRACT

These Image segmentation process includes image pre-processing, background removal, foreground detection, outlier removal and post processing. In order to develop an efficient image segmentation system, it is mandatory to design these sub-processes with utmost efficiency. Image segmentation systems can be designed to be application specific or application independent depending upon the design of these internal modules. Algorithms like kMeans, fuzzy C-Means, etc. are generic, but the output of these algorithms must be tuned depending upon the given application for efficient segmentation. For instance, in order to effectively segment leaf imagery, the output clusters of kMeans must be checked for green coloured values, and clusters where green colour is prominent must be extracted for segmentation. The same task can be done via the use of Saliency maps, Grey level co-occurrence integrated algorithm, etc. by tuning their internal parameters. Thus, there are a wide variety of similar algorithms developed In order to reduce this ambiguity, this text reviews different image segmentation algorithms, and compares their statistical performance in terms of peak-signal-to-noise-ratio (PSNR), delay needed for computation, minimum mean squared error (MMSE), most probable application, etc. Moreover, this text also evaluates certain nuances, advantages and drawbacks of these algorithms, which will assist researchers to select the best algorithm set based on their application. This text also recommends certain improvements which can be done in these algorithms, in order to improve their performance via fusion, cascading and ensembling.

Keywords: Image, segmentation, MMSE PSNR.

SAMRIDDHI : A Journal of Physical Sciences, Engineering and Technology, (2021); DOI : 10.18090/samriddhi.v13spli02.16

INTRODUCTION

Segmentation of images necessarily means extraction of image regions that are required for future processing in image processing applications like classification, clustering, disease identification, etc. In order to develop an effective image segmentation engine, it is necessary that pre-processing, filtering, enhancement, noise removal, background detection, foreground detection and outlier detection operations must be performed with high efficiency. The flow of these operations can be observed from the figure 1, wherein all the phases are connected in tandem for effective image segmentation. From the flow it can be observed that images are acquired from real time sources or taken from available datasets. Real-time image segmentation processes are complex when compared to dataset-based image segmentation ones, because real-time images have a largely varying number of noise sources, angular distortions, size variations, illumination variations, etc.

Corresponding Author : Prerna Pachunde, Deptt. of Electrical Engineering Department, Rajiv Gandhi College of Engineering Research and Technoology, Chandrapur India; e-mail : prerna.dahiwade@gmail.com

How to cite this article : Pachunde, P., Akojwar. S.G. (2021). Quantitative Analysis of Image Segmentation Algorithms: A Statistical Perspective.

SAMRIDDHI : A Journal of Physical Sciences, Engineering and Technology, Volume 13, Special Issue (2), 193-202

Source of support : Nil

Conflict of interest : None

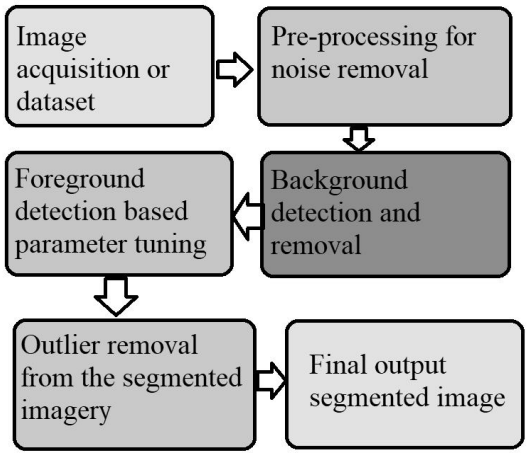

Figure 1: Flow of a typical image segmentation system

These images are given to a pre-processing block, wherein the following operations are performed [1],

- Noise removal using median filter, wiener filter, etc. in order to reduce the probability of distortions in the image. This is an essential process, and allows image to have clear visual components which makes the image easier to process by the consecutive blocks.
- Image enhancement via histogram equalization, colour palette modification, angular transforms, etc., which necessarily enhances regions of interest, while reducing the visual detail for background and outlier regions.
- Filtering image via registration, linear filters, non-linear filters, band pass filters, band stop filters, etc. is done such that the image is ready for background detection [2]. These filtering algorithms allow the image to be represented in a form where unwanted pixels have minimum entropy, while pixels coming under regions of interest have maximum entropy.

Once the pre-processing module has produced an image wherein background pixels have minimum entropy, while foreground pixels have maximum entropy, then background removal algorithms like quaternion detection, threshold-based filtering, etc. are applied. These algorithms aim at finding pixels which have minimum correlation and variance. Once these pixels are removed, then almost 60% segmentation process is complete, thus it is necessary that background detection algorithms must be designed with utmost efficiency. The following equation is followed for identification of background pixel probability,

$$BPP(x) = \frac{1}{k^2} * \int_{-k}^{k} \int_{-k}^{k} P_v(k,x)\, dx\ \ dx ....(1)$$

Where, 'k' is the neighbouring window size, ' ' is the pixel variance for the pixel number 'x'. Based on this probability, background pixels are removed, and the remaining pixels are passed to a foreground pixel identification block. This block is designed using saliency detection, entropy maximization, edge detection, texture analysis, thresholding, etc. The result of this block is a coarse segmented image, which consists of regions of interest, with some unwanted pixels a.k.a. outlier pixels. These outlier pixels are removed using the consequent block. The outlier removal block is also termed as post-processing block, which is designed depending upon the application. For instance, if the application demands extraction of fluid regions from brain MRI (Magnetic resonance imaging), then this block will remove all the grey and white regions from the foreground image regions, and present the remaining pixel-sets at the output. A large number of algorithms are designed by researchers over the years for segmentation of images, the next section reviews these algorithms, and suggests various optimizations that can be made in them in order to improve their efficiency. This is followed by statistical analysis of these algorithms w.r.t. their applicability. Finally, this text concludes with some interesting observations about these algorithms and suggests ways in which their performance can be optimized.

LITERATURE REVIEW

Image segmentation involves extraction of regions of interest from images such that these regions are useful for further image analysis. For instance, a brain magnetic resonance image (MRI) segmentation algorithm should be able to extract out the skull regions from the input image, such that these regions will be used to analyze presence of tumors or other disorders from the image. Such an algorithm that uses a modified version of fuzzy C-Means (FCM) can be observed from [2], wherein Pythagorean fuzzy sets are used in order to segment general purpose images. It uses a minimization objective function to reduce sum of every pixel to its clusters, the function can be observed from equation 2,

$$l_{x,y} = \sum_{i=1}^{m}\sum_{i=1}^{n} u_{ij}^2 * d^2(x_i, y_j).....(2)$$

Where, 'x' is the pixel value, 'y' is the cluster centre, 'd' is distance between pixel and cluster centre, while 'u' defines the fuzzy membership degree between pixel and cluster head, and (m, n) are the image size. The cluster centre is evaluated using the following equation,

$$y_i = \sum_{j=1}^{N} (u_{ij})^2 * x_{ij} / \sum_{j=1}^{N} (u_{ij})^2....(3)$$

Based on these equations, every image and its objective function values are evaluated. Based on the clusters where these values are minimum, image pixels are clustered into 1 of 'N' different parts. Each of these parts are represented using a different grey colour level in order to obtain the final segmentation results. A segmentation accuracy of 51% is achieved using this model, with a moderate delay of 272s for different images. This accuracy is high when compared with fuzzy C Means (FCM) that gives an accuracy of 46.6% and intuitionistic fuzzy C?means (IFCM) that gives an accuracy of 45.91%, but this accuracy is lower than kernel weighted fuzzy local information C-means (KWFLCM) which gives an accuracy of 53%. Although KWFLCM has good accuracy when compared with PFCM, but it requires an exponentially high delay of 4845 seconds, which is 17 times higher than the proposed PFCM method. This delay can be reduced and accuracy can be improved via the use of transfer learning as described in [3]. In this work, researchers have used object detection as the base model that performs effective image segmentation from the knowledge gained from transfer learning as observed from figure 2, wherein atrous spatial pyramid pooling (ASPP) is used for effective feature extraction.

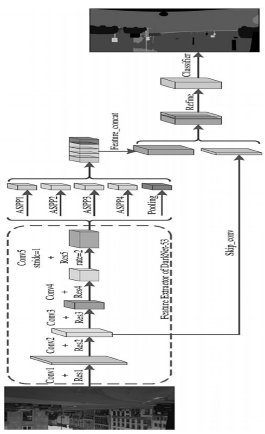

Figure 2: Transfer learning for image segmentation [3]

Due to this model an accuracy of 79.1% is achieved on ImageNet and COCO datasets. The model requires only 0.171 seconds for segmentation after training. The training delay is high, but is a one-shot operation, thus the average delay across multiple segmentation operations is low. This algorithm has higher accuracy when compared with DarkLab network which provides an accuracy of 76.3% and RefineNet which has an accuracy of 73.6%. But is has lower accuracy when compared with Pyramid Scene Parsing Network (PSPNet) which has an accuracy of 81.2%, and DeepLab Version 3, which has an accuracy of 82.1%. Both these models; even though have high accuracy, but are not tested on large image datasets, thus it is recommended that these models must be tested thoroughly before real-time deployment. A survey of such algorithms applied to different datasets can be observed from [4], wherein it is observed that convolutional neural network (CNN) based algorithms outperform other algorithms in terms of accuracy of segmentation and have reduced average delay of segmentation.

General purpose algorithms provide limited performance due to their application on a wide variety of applications, in order to improve this accuracy; application specific segmentation algorithms are developed via tuning the baseline algorithm's internal parameters. For instance, the work in [5] proposes a modified hybrid algorithm consisting of clustering, Bayesian classifier, and a Graph-based module for texture analysis in remote sensing images. The model uses mean approach for performing clustering, wherein mean red, green and blue values are evaluated for each window size. These values are evaluated using the following equation,

$$m_{(R/G/B)} = \frac{1}{N_c} * \sum_{i=1}^{N_c}\sum_{i=1}^{N_c} I_{(R/G/B)}(i, j).....(4)$$

Wherein, $m_{(R/G/B)}$ and $I_{(R/G/B)}$ are evaluated for each colour in the image, while N_c are number of pixels in the given window. Based on these values, clustering is performed. Optimization of the clustered pixels is done using average standard deviation values, which is evaluated using the following equation,

$$D_B = \sqrt{D_R^2 + D_G^2 + D_B^2}.....(5)$$

Where, D_R, D_G *and* D_B are average standard deviation values for the given colour sets.

Finally, a graph is created using these colour values and based on the edges and nodes of this graph image pixels are segmented. An accuracy of 90.82% is achieved using this hybrid method when tested on the LANDSAT dataset, which is higher than hierarchical weighted multi-segmenter (MW3AR) that has an accuracy of 88.01%, Dynamic hierarchical segmentation (DHC/K) that has an accuracy of 88.64 %, ENVI/M that has an accuracy of 86.48 %, Illumination invariant unsupervised segmenter (AR3D+EM) that has an accuracy of 86.59 %, Recursive texture fragmentation and reconstruction segmentation (R-TFR/F) that has an accuracy of 86.42 %, Unsupervised texture segmentation (TS-MRF/M) that has an accuracy of 86.98 % and tree-structured Markov random field model using Bayesian network (TS-MRF/K) that has an accuracy of 81.33 %. This improves the real-time applicability of the proposed method for satellite imagery. The performance of this algorithm can be improved by adding another layer of deep learning semantic model for segmentation as proposed in [6]. This model uses fast semantic image segmentation that assigns a class to each image pixel via a deep neural network. An aggregation of similar class pixels with a pre-decided confidence threshold results into the final segmented image. The proposed algorithm has a general-purpose accuracy of 71.65% which is evaluated for a large number of images. This accuracy can be further improved using a weakly supervised deep learning model as suggested in [7]. This model is applied to medical image segmentation and produces accuracies in the range of 98.9% for Trans rectal ultrasound scan (TRUS) images, 99.7% for computer tomography (CT) images and 98.8% for General-purpose ultrasound (US) images. Overall architecture for this highly accurate medical image segmentation model is observed , wherein a prior-knowledge generator block is used to generate initial segmentation maps. These maps are given to a segmentation block in order to obtain the final segmented image. Other approaches for medical image segmentation are described in [8], from where it can be observed that deep neural network based on VGGNet architecture outperforms other algorithms by providing an accuracy of 85.5% across 14,696 image scans. Fusion of the model in [7] and [8] can be done in order to effectively segment lung regions with high accuracy. In order to perform this fusion, the work in [9] can be used. This work is based on an altogether different domain of petrochemical sensors, but the baseline algorithm can be used for fusion of any two methods.

Another application specific image segmentation model that is capable of detecting raw G-band chromosomes from genetic sequence images can be observed from [10]. In this model a decision tree algorithm is used which is based on thresholding in order to obtain an accuracy of 96% for different chromosome segmentation applications. The decision tree is based on image parameters like Object size, Maximum single chromosome size, Object pixel intensity, Thickness throughout the skeleton, Average thickness, Number of end points and Number of branch points. These parameters are given to a thresholding unit in order to separate out a single chromosome (T-cell) from the entire image. The model was tested on 508 images, and highly accurate results were evaluated. But this accuracy might reduce as number of images used for testing are increased. In order to keep a consistency in accuracy of segmentation, the work in [11] proposes a gradient-based oriented distance evaluation model, that uses gradient direction information from edge data in order to improve clustering performance for image pixels. This model reduces overall computation time by 15% and produces an accuracy of 85% for traffic sign and number plate images, which is moderate, but can be used for real-time deployments.

A large variety of noise types can affect the image while it is undergoing segmentation. These noise types are also called as noise artefacts, and affect segmentation performance. In order to correct these artefacts, work in [12] suggests a deep learning model which is uses time displaced line detection features in order to reduce detection loss, reconstruction loss and segmentation loss in the segmented image. This network is attached to reconstruction and segmentation CNN models to perform high accuracy segmentation via network cascading. It is observed that the proposed cascaded CNN model is able to achieve a segmentation accuracy of 96.2%, which is high when compared with dual channel CNN which has an accuracy of 90.8%, single-channel CNN that has an accuracy of 94.8%, and baseline CNN model that has an accuracy of 93.2%, thereby making the proposed model highly effective for both noise removal and high accuracy segmentation applications.

Transfer learning approaches allow the knowledge gained from one domain to be used in another domain without the need of retraining the network. The work in [13] proposes such an algorithm

that uses a combination of kernel learning and image weighting in order to reduce maximum mean discrepancy (MMD) for joint kernel optimization. The model is applied on MRI images, and produces an accuracy of 80%, which can be useful for high-speed segmentation applications. Transfer learning models can use fuzzy clustering in order to improve their efficiency, which can be observed from [14], wherein a comparison of different fuzzy clustering models is applied on MRI images, and their performance is evaluated. It is observed that extended Fuzzy C-Means (eFCM) model that uses a combination of image enhancement and FCM outperforms other fuzzy-based segmentation methods. The model reduces noise and enhances image quality using the following equation,

$$I_{l,m,e} = \sum_{e=1}^{8}\left(\frac{1}{N}\right)*\left(\left(\sum_{i=l-1}^{l+1}\sum_{j=m-1}^{m+1} I(i,j,e)\right) - I_{l,m,e}\right) ..(6)$$

Where, the image dimensions are depicted using (l, m, n) and the image is represented using 'I'. Due to this equation, noise components from the image are reduced, thereby resulting into an accuracy of 95.1% when compared on different image types, which is higher than FCM (79.1%), Credibilistic FCM (54.2%), FCM type 2 (20.8%), Kernel-based FCM (78%), Intuitionistic FCM (78.26%), Kernel-based Intuitionistic FCM (65.2%), Credibilistic Kernel-based FCM (51.28%) and Credibilistic Intuitionistic FCM (64.9%) models.

Semantic segmentation models are also used for performing high accuracy image segmentation. The work in [15] proposes such a CNN-based semantic segmentation model that is applied on scanning electron microscopy (SEM) imagery. The algorithm uses pixel-level contextual class annotations, damage v/s background segmentation, contextual semantic segmentation and visual inspection blocks in order to generate class-level masks. These masks are given to a CNN-based U-Net and Seg-Net architecture in order to improve segmentation performance of the system. The system is able to achieve an accuracy of over 85% when applied to segmentation of damage in concrete images. This performance can be further enhanced via the use of adaptive morphological reconstruction (AMR), wherein noise removal can be done via removal of unwanted seed points, use of multi-scale structuring elements and hierarchical segmentation as suggested in [16].

The algorithm is able to improve accuracy of original seeded region growing (SRG) algorithm from 71% to 80% when compared on a large set of images. This accuracy can be further enhanced with the help of multi-task deep learning models which use fully convolutional network (FCN) architectures for segmentation. Such a model can be observed from [17] wherein 3D images are segmented using Simultaneous Segmentation and Landmark Localisation Network (SSLLN). This network is applied to cardiac images in order to obtain an accuracy of 94.3% which makes it suitable for real-time clinical use. This accuracy is high when compared with 3D Seg CNN (92.3%), 3D-Auto Encoder (92.6%) and 3D anatomically constrained neural network model (93.9%), thereby making it useable for real-time deployments. The accuracy of this model can be improved by addition of a boundary-weighted domain adaptive neural network (BOWDANet) as described in [18], wherein an accuracy of 95.5% is achieved for MRI images. Another application specific image segmentation model based on two-stage CNN models for Spinal cord segmentation can be observed from [19], wherein semantic image classification is used. This model has an accuracy of 87.32% for segmenting spinal cord data from over 500 images, which makes it useful for clinical deployments. The architecture uses a combination of graph convolutional segmentation network (GCSN) and residual U-Net (ResUNet) for coarse and fine segmentation respectively, due to which such a high accuracy is achieved. Other measures for evaluating performance of image segmentation models can be observed in [20], wherein White Matter Hyperintensities (WMH) segmentation is used as an application for evaluation of metrics like Dice similarity coefficient, absolute log-transformed volume difference, modified Hausdorff distance (95th percentile), F1-score andsensitivity. These measures can be used for evaluating performance of any kind of image segmentation models.

The Bayesian UNet model which is similar to hyper-dense model is described in [21] also provides good segmentation accuracy of 84% on both medical and general-purpose datasets. These models have good accuracy when input images are of good quality, but as the input image quality deteriorates, so does the accuracy of segmentation. In order to achieve high image segmentation accuracy for low contrast images a high-resolution encoder-decoder combination is described in [22]. This model uses a

combination of skipped connections along with high resolution pathways that are deeply supervised, and guided via minimization of cross-entropy and contour regression models to improve edge detection quality.

Due to this high-resolution pathway and the use of encoder-decoder network, an accuracy of 89% is achieved for prostate, bladder and other medical image segmentation applications. Other architectures like the ones mentioned in [23], [24], [25] and [26] use similar deep learning approaches like Markov Random Fields, Locally-Oriented Appearance and Dictionary Learning, Fully Connected Network (FCN) and Hausdorff Distance minimized CNN respectively. These architectures are able to obtain an accuracy of 78.9%, 95%, 82.08% and 96% respectively on different medical domain applications.

A novel work that uses domain-oriented feature embedding (DoFE) for segmentation of unknown medical images is proposed in [27]. This model uses aggressively domain specific feature sets in order to improve the efficiency of segmentation, and uses these feature sets in order to create a Domain Knowledge Pool (DKP). Features from new images are matched with this DKP, and depending upon matching percentages, application specific segmentation is performed. An accuracy of 88.44% is achieved using this model, which is high enough for clinical use. The model is tested only for fundus images, and must be tested for a larger number of domains for better performance evaluation. Transfer learning model like the one mentioned in [28] can also be used to improve its accuracy, wherein DKP can be created for one domain and used for another domain for reducing training delay. The transfer learning model of [38] is able to achieve accuracies in the range of 98% for medical segmentation, and thus; must be tested for non-medical domains as well. Similar models are mentioned in [29], [30], [31] and [32] wherein deep attentive features, generative adversarial model, Fully Convolution Network with Continuous Max-Flow, Deep Neural Network Regression and Anatomy-Regularized Representation Learning are used for enhancing medical image segmentation accuracy. These models have an accuracy of 90%, 85%, 93.2%, 96.6% and 81.05% respectively for different medical applications. As these models are based on CNN and its sub-types, it is observed that their performance is better than their non-CNN counterparts. In order to evaluate performance of these models, the next section compares these models in terms of accuracy, application and computation complexity which is directly proportional to delay of execution. This comparison will assist researchers to identify best possible algorithm set(s) for their specific applications, which will not only reduce the time needed for deployment, but also guarantee an optimal system performance.

STATISTICAL ANALYSIS

In order to compare performance of the reviewed algorithms, these algorithms are evaluated in terms of overall accuracy (Acc.), application (App.) and computational complexity (CC). The computational complexity is converted into complexity levels from 1 to 5, wherein each of these values are inferred from the following table-1.

Table-1: Computational Complexity to Computational Level Inference

Computational Complexity	Complexity Level
O (1)	1
O (n)	2
O (n*log(n))	3
O (n^c)	4
O (n!)	5

Based on this inference, the following comparison shown in table-2 is done for each of the reviewed algorithms.

Table-2: Application Specific Performance Evaluation of Different Algorithms

Method	App.	Acc. (%)	CC
PFCM [2]	General	51	3
FCM [2]	General	46.6	2
IFCM [2]	General	45.9	2
KWFLCM [2]	General	53	5
CNN with ASPP with TL [3]	General	79.1	4
DarkLab [3]	General	76.3	4
RefineNet [3]	General	73.6	4
PSPNet [3]	General	81.2	5
DeepLab [3]	General	82.1	5
Hybrid GBBT [5]	Satellite	90.8	4
MW3AR [5]	Satellite	88.01	3
DHC/K [5]	Satellite	88.64	3
ENVI/M [5]	Satellite	86.48	4
AR3D+EM [5]	Satellite	86.59	4
R-TFR/F [5]	Satellite	86.42	3
TS-MRF/M [5]	Satellite	86.98	4
TS-MRF/K [5]	Satellite	81.33	4

Fast Semantic [6]	General	71.65	5
Weakly supervised DL [7]	Medical	98.9	5
VGGNet CNN [8]	General	85.5	4
DT [10]	Medical	96	4
GB ODE [11]	General	85	3
CRNN Noise Removal [12]	Medical	96.2	5
Dual CNN [12]	Medical	90.8	4
Single channel CNN [12]	Medical	94.8	4
GoogLeNet CNN [12]	Medical	93.2	4
MMD with TL [13]	Medical	80	3
eFCM [14]	General	95.1	2
FCM [14]	General	79.1	2
FCM T2 [14]	General	20.8	1
CFCM [14]	General	54.2	2
KFCM [14]	General	78	3
IFCM [14]	General	78.26	3
KIFCM [14]	General	65.2	3
CKFCM [14]	General	51.28	3
CIFCM [14]	General	64.9	3
CNN UNet and SegNet [15]	Medical	85	4
AMR with SRG [16]	General	74	3
SSLLN [17]	Medical	94.3	5
3D Seg CNN [17]	Medical	92.3	4
3D AE [17]	Medical	92.6	4
3D ACNN [17]	Medical	93.9	5
BOWDANet [18]	Medical	95.5	5
GCSN with ResUNet [19]	Medical	87.3	4
GAN [21]	Medical	85.66	5
3D UNet [21]	Medical	77.41	4
Deep Support GAN [21]	Medical	77.82	5
Two-stage CNN [21]	Medical	83.85	5
VGGNet [22]	General	96.6	4
Weakly Supervised CNN [23]	General	85	5
2D and 3D CNN [24]	General	88.4	5
CA CNN [25]	General	87.08	5
3D APA CNN [26]	General	94.1	5
UNet++ [27]	General	97.81	5
Key point CNN [29]	Multi modal	50	4
Hyper dense networks [30]	Multi modal	95.8	5
Connection less Single path [30]	Multi modal	90.1	4
Connection less dual-path [30]	Multi modal	94.82	5
Connected dual-path [30]	Multi modal	95.5	5
Bayesian UNet [31]	Multi modal	84	4
High resolution encoder decoder [32]	Medical	89	5
Markov Random Fields [33]	Medical	78.9	3
Locally-Oriented Appearance and Dictionary Learning [34]	Medical	95	4
FCN [35]	Medical	82.08	4
HD CNN [36]	Medical	96	5
DoFE CNN [37]	Medical	88.44	4
3D ACNN [17]	Medical	93.9	5
BOWDANet [18]	Medical	95.5	5
GCSN with ResUNet [19]	Medical	87.3	4
GAN [21]	Medical	85.66	5
3D UNet [21]	Medical	77.41	4
Deep Support GAN [21]	Medical	77.82	5
Two-stage CNN [21]	Medical	83.85	5
VGGNet [22]	General	96.6	4
Weakly Supervised CNN [23]	General	85	5
2D and 3D CNN [24]	General	88.4	5
CA CNN [25]	General	87.08	5
3D APA CNN [26]	General	94.1	5
UNet++ [27]	General	97.81	5
Key point CNN [29]	Multi modal	50	4
Hyper dense networks [30]	Multi modal	95.8	5
Connection less Single path [30]	Multi modal	90.1	4
Connection less dual-path [30]	Multi modal	94.82	5
Connected dual-path [30]	Multi modal	95.5	5
Bayesian UNet [31]	Multi modal	84	4
High resolution encoder decoder [32]	Medical	89	5
Markov Random Fields [33]	Medical	78.9	3
Locally-Oriented Appearance and Dictionary Learning [34]	Medical	95	4
FCN [35]	Medical	82.08	4
HD CNN [36]	Medical	96	5
DoFE CNN [37]	Medical	88.44	4

From this performance evaluation, it is observed that these algorithms are majorly used for Medical, Multimodal, Satellite or General-purpose applications. Thus, in order to assist researchers to effectively select these algorithms, the following figures 3, 4, 5, and 6 are used. These figures compare accuracy of reviewed algorithms w.r.t. their application of use.

From these figures it can be observed that CNN-based models outperform other models in terms of raw accuracy of segmentation, but these algorithms have high complexity of execution due to which high performance processing elements are needed for implementation. Moreover, these algorithms can be optimized using transfer learning models for improved speed.

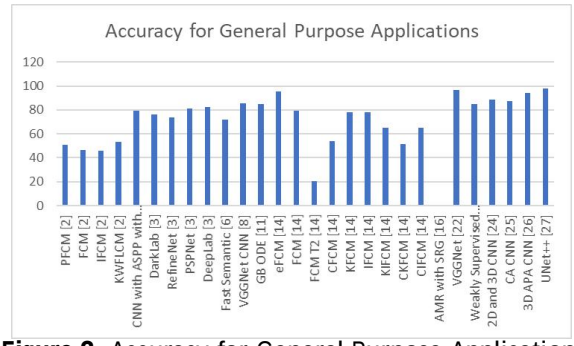

Figure 3: Accuracy for General Purpose Applications

For general purpose applications, it can be observed that UNet++, eFCM and VGGNet based CNN models outperform other models, thus they can be used for high performance segmentation. Similarly, medical image segmentation algorithms can be observed from figure 4 as follows,

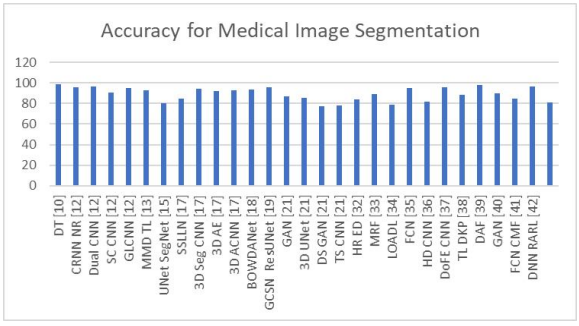

Figure 4: Accuracy for Medical Image Segmentation

For medical imaging applications, it can be observed that most algorithms give very good segmentation results, but architectures like Decision Tree [33], CRNN Noise Removal [34] and DAF [35] models outperform other models, thus they can be used for high performance segmentation. Similarly, multimodal image segmentation algorithms can be observed from figure 5, wherein image segmentation is performed in order to extract multiple regions of interest from the input image

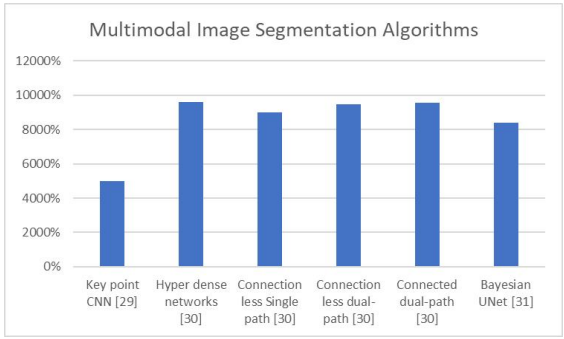

Figure 5: Accuracy for Multimodal Segmentation

For multimodal applications, it can be observed that Hyper dense networks [36] [37] outperform other models, thus they can be used for high performance segmentation. Similarly, satellite image segmentation

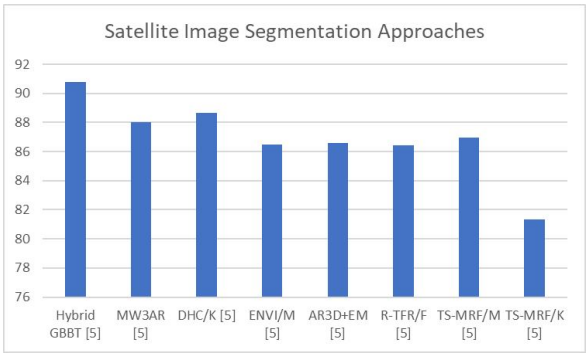

Figure 6: Accuracy for Satellite image segmentation

algorithms can be observed from figure 6 as follows,

For satellite image segmentation, it can be observed that Hybrid GBBT outperforms other models, thus they can be used for high performance segmentation. This inference will be useful for researchers in order to select the most suited algorithm for their given application.

Conclusion and Future Scope

From the result evaluation, it can be observed that CNN and its related models outperform other models in terms of core accuracy of segmentation. For general purpose applications like natural image segmentation, object-based segmentation, etc. the eFCM model and VGGNet models are highly recommended due to their high accuracy and low complexity, while the UNet++ model can be used for highly precise segmentations. Other applications like satellite image segmentation & multimodal segmentation requires high complexity algorithms like Hybrid GBBT and Hyperdense networks respectively in order to obtain high segmentation accuracy. Medical imaging algorithms are already saturated in terms of accuracy, and use models like transfer learning, GAN and other CNN types in order to obtain high accuracy of segmentation. It is recommended that eFCM be integrated with CNN models, and transfer learning be used for inter-domain knowledge transfer in order to achieve high quality multi-domain segmentation.

REFERENCES

[1] survey of image segmentation: clustering methods, performance parameters, and benchmark datasets. Multimed Tools Appl (2021). https://doi.org/10.1007/s11042-021-10594-9

[2] Ma, R, Zeng, W, Song, G, Yin, Q, Xu, Z. Pythagorean fuzzy C means algorithm for image segmentation. Int J Intell Syst. 2021; 36: 1223 1243. https://doi.org/10.1002/int.22339

[3] Zhang, WJ, Chen, Z, Xu, Z. An efficient semantic segmentation method based on transfer learning from object detection. IET Image Process. 2021; 15: 57– 64. https://doi.org/10.1049/ ipr2.12005

[4] Ramadan, H., Lachqar, C. &Tairi, H. A survey of recent interactive image segmentation methods. Comp. Visual Media 6, 355–384 (2020). https://doi.org/10.1007/s41095-020-0177-5

[5] Song, Y., Qu, J. Real-time segmentation of remote sensing images with a combination of clustering and Bayesian approaches. J Real-Time Image Proc (2020). https://doi.org/10.1007/s11554-020-00990-z

[6] He, D., Xie, C. Semantic image segmentation algorithm in a deep learning computer network. Multimedia Systems (2020). https://doi.org/10.1007/s00530-020-00678-1

[7] Girum, K.B., Créhange, G., Hussain, R. et al. Fast interactive medical image segmentation with weakly supervised deep learning method. Int J CARS 15, 1437–1444 (2020). https://doi.org/10.1007/s11548-020-02223-x

[8] Sinha, P., Tuteja, M. &Saxena, S. Medical image segmentation: hard and soft computing approaches. SN Appl. Sci. 2, 159 (2020). https://doi.org/10.1007/s42452-020-1956-4

[9] Xiong, Jianbin& Zhang, Qinghua& Peng, Zhiping& Sun, Guoxi&Cai, Yongda. (2016). Double Sample Data Fusion Method Based on Combination Rules. IEEE Access. PP. 10.1109/ACCESS.2016.2604824.

[10] Altinsoy, E., Yang, J. and Yilmaz, C. (2020), Fully automatic raw G band chromosome image segmentation. IET Image Processing, 14: 1920-1928. https://doi.org/10.1049/iet-ipr.2019.1104

[11] Li, Chunming & Xu, Chenyang&Gui, Changfeng& Fox, M.D.. (2011). Distance Regularized Level Set Evolution and Its Application to Image Segmentation. Image Processing, IEEE Transactions on. 19. 3243 - 3254. 10.1109/TIP.2010.2069690.

[12] Oksuz, Ilkay & Clough, James &Ruijsink, Bram &Puyol Anton, Esther &Bustin, Aurélien & Cruz, Gastao& Prieto, Claudia & King, Andrew & Schnabel, Julia. (2020). Deep Learning Based Detection and Correction of Cardiac MR Motion Artefacts During Reconstruction for High-Quality Segmentation. IEEE Transactions on Medical Imaging. PP. 1-1. 10.1109/TMI.2020.3008930.

[13] A. Van Opbroek, H. C. Achterberg, M. W. Vernooij and M. De Bruijne, "Transfer Learning for Image Segmentation by Combining Image Weighting and Kernel Learning," in IEEE Transactions on Medical Imaging, vol. 38, no. 1, pp. 213-224, Jan. 2019, doi: 10.1109/TMI.2018.2859478.

[14] Kaur, P, Sharma, P, Palmia, A. Fuzzy clustering based image segmentation techniques used to segment magnetic resonance imaging/computed tomography scan brain tissues: Comparative analysis. Int J Imaging Syst Technol. 2020; 30: 1294– 1323. https://doi.org/10.1002/ima.22439

[15] BAJCSY, P., FELDMAN, S., MAJURSKI, M., SNYDER, K. and BRADY, M. (2020), Approaches to training multiclass semantic image segmentation of damage in concrete. Journal of Microscopy, 279: 98-113. https://doi.org/10.1111/jmi.12906

[16] T. Lei, X. Jia, T. Liu, S. Liu, H. Meng and A. K. Nandi, "Adaptive Morphological Reconstruction for Seeded Image Segmentation," in IEEE Transactions on Image Processing, vol. 28, no. 11, pp. 5510-5523, Nov. 2019, doi: 10.1109/TIP.2019.2920514.

[17] J. Duan et al., "Automatic 3D Bi-Ventricular Segmentation of Cardiac Images by a Shape-Refined Multi- Task Deep Learning Approach," in IEEE Transactions on Medical Imaging, vol. 38, no. 9, pp. 2151-2164, Sept. 2019, doi: 10.1109/TMI.2019.2894322.

[18] Zhu, Qikui& Du, Bo & Yan, Pingkun. (2019). Boundary-weighted Domain Adaptive Neural Network for Prostate MR Image Segmentation.

[19] S. Pang et al., "SpineParseNet: Spine Parsing for Volumetric MR Image by a Two-Stage Segmentation Framework With Semantic Image Representation," in IEEE Transactions on Medical Imaging, vol. 40, no. 1, pp. 262-273, Jan. 2021, doi: 10.1109/TMI.2020.3025087.

[20] Kuijf, Hugo &Biesbroek, Matthijs& de Bresser, Jeroen & Heinen, Rutger & Andermatt, Simon & Bento, Mariana &Berseth, Matt &Belyaev, Mikhail & Cardoso, Manuel Jorge & Casamitjana, Adrià& Collins, Louis &Dadar, Mahsa& Georgiou, Achilleas & Ghafoorian, Mohsen &Jin, Dakai&Khademi, April & Knight, Jesse & Li, Hongwei&Llado, Xavier &Biessels, Geert. (2019). Standardized Assessment of Automatic Segmentation of White Matter Hyperintensities; Results of the WMH Segmentation Challenge. IEEE Transactions on Medical Imaging. PP. 1-1. 10.1109/TMI.2019.2905770.

[21] X. Chen et al., "One-Shot Generative Adversarial Learning for MRI Segmentation of Craniomaxillofacial Bony Structures," in IEEE Transactions on Medical Imaging, vol. 39, no. 3, pp. 787-796, March 2020, doi: 10.1109/TMI.2019.2935409.

[22] Q. Meng et al., "Weakly Supervised Estimation of Shadow Confidence Maps in Fetal Ultrasound Imaging," in IEEE Transactions on Medical Imaging, vol. 38, no. 12, pp. 2755-2767, Dec. 2019, doi: 10.1109/TMI.2019.2913311.

[23] M. Li et al., "Image Projection Network: 3D to 2D Image Segmentation in OCTA Images," in IEEE Transactions on Medical Imaging, vol. 39, no. 11, pp. 3343-3354, Nov. 2020, doi: 10.1109/TMI.2020.2992244.

[24] S. Pang et al., "Hippocampus Segmentation Based on Iterative Local Linear Mapping With Representative and Local Structure-Preserved Feature Embedding," in IEEE Transactions on Medical Imaging, vol. 38, no. 10, pp. 2271-2280, Oct. 2019, doi: 10.1109/TMI.2019.2906727.

[25] CA-Net: Comprehensive Attention Convolutional Neural Networks for Explainable Medical Image Segmentation, https://arxiv.org/abs/2009.10549

[26] H. Jia et al., "3D APA-Net: 3D Adversarial Pyramid Anisotropic Convolutional Network for Prostate Segmentation in MR Images," in IEEE Transactions on Medical Imaging, vol. 39, no. 2, pp. 447-457, Feb. 2020, doi: 10.1109/TMI.2019.2928056.

[27] UNet++: Redesigning Skip Connections to Exploit Multiscale Features in Image Segmentation, https://arxiv.org/abs/1912.05074

[28] L. Wang et al., "Benchmark on Automatic Six-Month-Old Infant Brain Segmentation Algorithms: The iSeg-2017 Challenge," in IEEE Transactions on Medical Imaging, vol. 38, no. 9, pp. 2219-2230, Sept. 2019, doi: 10.1109/TMI.2019.2901712.

[29] C. Wachinger, M. Toews, G. Langs, W. Wells and P. Golland, "Keypoint Transfer for Fast Whole-Body Segmentation," in IEEE Transactions on Medical Imaging, vol. 39, no. 2, pp. 273-282, Feb. 2020, doi: 10.1109/TMI.2018.2851194.

[30] J. Dolz, K. Gopinath, J. Yuan, H. Lombaert, C. Desrosiers and I. Ben Ayed, "HyperDense-Net: A Hyper-Densely Connected CNN for Multi-Modal Image Segmentation," in IEEE Transactions on Medical Imaging, vol. 38, no. 5, pp. 1116-1126, May 2019, doi: 10.1109/TMI.2018.2878669.

[31] Seeböck, Philipp & Orlando, José &Schlegl, Thomas &Waldstein, Sebastian &Bogunoviæ, Hrvoje&Riedl, Sophie &Langs, Georg & Schmidt-Erfurth, Ursula. (2019). Exploiting Epistemic Uncertainty of Anatomy Segmentation for Anomaly Detection in Retinal OCT. IEEE Transactions on Medical Imaging. PP. 1-1. 10.1109/TMI.2019.2919951.

[32] S. Zhou, D. Nie, E. Adeli, J. Yin, J. Lian and D. Shen, "High-Resolution Encoder–Decoder Networks for Low-Contrast Medical Image Segmentation," in IEEE Transactions on Image Processing, vol. 29, pp. 461-475, 2020, doi: 10.1109/TIP.2019.2919937.

[33] R. Bates et al., "Segmentation of Vasculature From Fluorescently Labeled Endothelial Cells in Multi-Photon Microscopy Images," in IEEE Transactions on Medical Imaging, vol. 38, no. 1, pp. 1-10, Jan. 2019, doi: 10.1109/TMI.2017.2725639.

[34] Onofrey, John &Staib, Lawrence &Papademetris, Xenophon. (2018). Segmenting the Brain Surface From CT Images With Artifacts Using Locally Oriented Appearance and Dictionary Learning. IEEE Transactions on Medical Imaging. PP. 1-1. 10.1109/TMI.2018.2868045.

[35] Ren, Xuhua& Zhang, Lichi& Ahmad, Sahar &Nie, Dong & Yang, Fan & Xiang, Lei & Wang, Qian. (2019). Task Decomposition and Synchronization for Semantic Biomedical Image Segmentation.

[36] D. Karimi and S. E. Salcudean, "Reducing the Hausdorff Distance in Medical Image Segmentation With Convolutional Neural Networks," in IEEE Transactions on Medical Imaging, vol. 39, no. 2, pp. 499-513, Feb. 2020, doi: 10.1109/TMI.2019.2930068.

[37] S. Wang, L. Yu, K. Li, X. Yang, C. -W. Fu and P. -A. Heng, "DoFE: Domain-Oriented Feature Embedding for Generalizable Fundus Image Segmentation on Unseen Datasets," in IEEE Transactions on Medical Imaging, vol. 39, no. 12, pp. 4237-4248, Dec. 2020, doi: 10.1109/TMI.2020.3015224.